

In-situ Detection of Build Defects in Additive Manufacturing via Impedance-Based Monitoring

Logan Sturm¹, Mohammed Albakri², Dr. Christopher B. Williams¹, Dr. Pablo Tarazaga²

¹ Design, Research, and Education for Additive Manufacturing Systems Lab

² Vibrations, Adaptive Structures and Testing Laboratory

Department of Mechanical Engineering, Virginia Polytechnic and State University

Abstract

In this paper, the authors explore the use of impedance-based monitoring techniques for the in-situ detection of additive manufacturing build defects. By physically coupling a piezoceramic (PZT) sensor to the part being fabricated, the measured electrical impedance of the PZT can be directly linked to the mechanical impedance of the part. It is hypothesized that one can detect in-situ defects of part mass and stiffness by comparing the signatures collected during printing of parts with that of a defect-free control sample. In this paper, the authors explore the layer-to-layer sensitivity of this technique. A control sample is created using Material Jetting and the change in signatures between various layer intervals is measured. To evaluate the technique's ability to perform in-situ detection, several parts containing designed defects (e.g., internal voids) are fabricated and their layer-to-layer signatures are compared to a control sample. Using this technique, the authors demonstrate an ability to track print progress and detect defects as they occur.

1. Introduction

With the development and maturation of additive manufacturing (AM) there are an increasing number of end use products being fabricated with these technologies. This shift from producing prototypes to fabricating functional end-use products has created a growing need for part validation and quality control [1]. Defects or process variations that might be acceptable in a demonstrational, tooling, or prototype part are no longer acceptable in an end use product. In particular, the aerospace industry has begun to adopt AM technologies for the fabrication of high value, low volume parts. Some example of AM parts being produced and tested include direct printed metals (e.g., Rolls Royce Trent-XWB bearing (Figure 1a) and RUAG's Sentinel satellite bracket (Figure 1b)) and polymers (e.g., FAA-approved ULTEM 9085 aircraft air duct created by Stratasys and Orbis (Figure 1c)).



(a) Rolls Royce Trent-XWB bearing [2] (b) RUAG's Sentinel satellite bracket [3] (c) Stratasys/Orbis' conformal air duct [4]

Figure 1. Example applications of AM to fabricate mission-critical aerospace components.

1.2 In-situ Monitoring for Additive Manufacturing

In their *Measurement Science Roadmap for Metal-based Additive Manufacturing*, NIST states that “Existing NDE techniques are not optimized for AM processes, materials or parts. Techniques are lacking for in-situ NDI, and post-process AM part inspection.” [1]. To address the needs presented by NIST, the authors suggest that an ideal in-situ NDE technique for AM would have the following attributes:

- Cost-effective.
- Able to be conducted quickly.
- Able to evaluate parts irrespective of geometry and material. In other words, the technique would be able to analyze inaccessible features, large parts, fine features, rough surface finish, etc.
- Able to detect both surface and internal defects. In particular, the ability to detect changes in non-surface material properties that may occur due to factors such as thermal effects during or after the fabrication of subsequent layers.

In addition to this, the authors propose that an ideal method would be resistant to cyber-attacks. As discussed in their previous work [5], there are variety of cyber-physical vulnerabilities that exist in quality control (QC) and AM due to the digital nature of the process chain. Since a Stuxnet-style attack that compromises a printer could compromise the sensors on the printer as well, it is advantageous to have independent side-channel measurements that can monitor the part fabrication independently from the printer.

Current in-situ monitoring approaches have focused on the performance of direct metal systems such as SLM and LENS. A variety of approaches have be presented in research such as high-speed cameras [6], thermocouples, pyrometers [7, 8]. These techniques are limited to the

inspection of the surface geometry of a part. Other methods of inspection have been considered, such as neutron diffraction and X-ray backscatter [9]. The methods can detect defects volumetrically, but require expensive radiation sources. Laser ultrasonic testing has also been investigated as a way of detecting surface defects and has some capability to detect volumetric properties such as thickness [10]. Many in-situ systems focus on monitoring the melt pool instead of the entire build area since this allows for increased resolution. One method presented by Lott et al. is through the use of an illumination laser in combination with a high-speed camera [11]. While this allows for precise monitoring of the melt pool it is not able to monitor the entire build area or to detect thermal changes that may occur in previous layers as a result of the heating of already fabricated layers during the fabrication of new layers.

Some work outside of direct metal AM has been performed using a variety of sensors and the use of data fusion to integrate their results together. Rao et al. demonstrated the use of thermocouples, accelerometers, an IR temperature sensor, and a borescope to monitor and detect build defects in an FDM process [12]. The primary focus of in-situ monitoring so far has been on monitoring either the build layer or the machine behavior. In the first case, the primary concern is with tracking the geometry of the part or with monitoring the thermal characteristics to model the behavior of the system. While these methods are useful, they lack the ability to directly measure the material properties and are limited to monitoring the surface of the part. In the second case the focus is on detecting when the machine is operating outside of normal parameters (indicating a build failure). While this method provides valuable feedback information, it does nothing to directly monitor the properties of the part.

1.3 Research Goal

Based on the previous work that has been done in in-situ monitoring, the authors believe that there is still a need for an in-situ monitoring technique that is able to directly interrogate the material properties and geometry of the part being fabricated. The overall goal of this paper is to assess the feasibility of using in-situ electromechanical impedance measurements for NDE of additively manufactured parts. The authors' previous work has established that piezo-ceramics sensors can be used as a post-process NDE tool to detect defects in fully fabricated AM parts [13]. Based on this work, the authors believe that impedance based measurements may have potential for in-situ monitoring as well. The use of these sensors in-situ poses new challenges. One concern is that, since the part is attached to a build plate during fabrication, the impedance response due to the much larger mass of the machine may overwhelm the relatively small mass of the fabricated part, which could result in defects being undetectable. Another concern is that vibrations from the machine might influence the sensor reading, resulting in a poor signal to noise ratio. Finally, there is the concern that the location of a part on the build tray might affect the measurement, and thus prevent successful comparison of the measurements between different parts. To evaluate if impedance-based measurements via piezo-ceramics are a valid method for in-situ AM measurement, the authors sought to verify the following hypotheses:

1. For a single part at a given layer, the sensors will be able to repeatedly measure the same signature.
2. For a single part, the sensors will be able to detect the change from one layer to another. This change will be greater than the signature variation in a single layer.
3. While being fabricated, all parts will have similar signatures until the defects occur. After the defects are introduced, the sensors will be able to detect differences in the parts' signatures.

To verify these hypotheses, the authors designed and printed a series of test specimens which contain internal build errors (as described in Section 3.1). Impedance measurements were conducted and compared against a set of defect-free parts (Section 3.2). Results from this comparison are presented and analyzed in Section 4. Closure and future work are presented in Section 5.

The need for reliable methods of verifying the quality of AM parts presents a significant barrier to widespread industrial adoption of AM technologies. Before AM parts can be adopted in end use and mission critical roles reliable methods of certification are needed. While some existing methods such as X-ray CT have been able to provide validation for existing parts, these methods are expensive and new designs are pushing the size limits of current scanners. Several organizations such as NIST [1], NASA [14], and the ASTM F-42 committee [15] have recognized the need for NDE techniques optimized for AM.

To address this research gap, the authors propose the use of electromechanically impedance measurements as a means to detect and identify AM defects. The authors' previous work has demonstrated this potential with fully fabricated part and the authors seek to extend this work to in-situ monitoring. By monitoring parts in-situ defects are able to be detected sooner allowing for reduced waste and potentially the repair of defects before they become internal to the part. A detailed overview of impedance-based SHM and its extension to NDE of AM parts is provided in Section 2.

2.0 Non-Destructive Evaluation for Additive Manufacturing

2.1 Electromechanical Impedance for SHM and NDE

The basis for using electromechanical impedance for structural health monitoring or non-destructive evaluation is the impedance signature that a part will have. Each part has a unique combination of mass, stiffness, and damping characteristics that result in a unique dynamic response (impedance signature). If damage occurs to the part or a defect is introduced these part characteristics will change, altering the dynamic response. In impedance based SHM has shown potential as a real time damage assessment method that is non-intrusive, cost effective, and highly sensitive [16]. This technique utilizes piezoelectirc materials, specifically lead zirconate titanate (PZT) wafers as both the sensor and the actuator to both excite the structure and measure its response [17,18]. By attaching these sensors to the part, the mechanical properties of the part

are coupled with the electrical properties of the sensor, allowing the measurement of the mechanical impedance of the part to be simplified to the measurement of the electrical impedance of the sensor which is directly related. The electrical impedance of the piezo can be easily measured, allowing changes in the mechanical impedance to be detected. This allows changes in the part characteristics due to factors such as build defects to be detected by changes in the electrical impedance signature [17, 18].

Figure 2 shows a schematic of a piezoelectric patch attached to a printed part, which is represented by an equivalent spring, mass, and damper system. Assuming linear piezoelectricity, the constitutive equations of the piezoelectric materials operating in 1-3 mode can be expressed as [19]

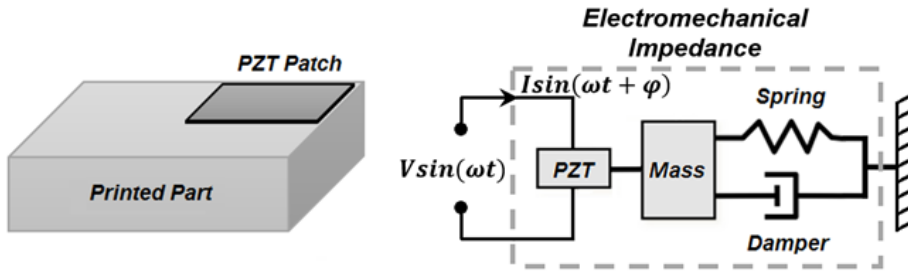


Figure 2. A piezoelectric patch attached to a mechanical structure represented by a spring-mass-damper system.

$$\begin{aligned} \varepsilon_{11} &= s_{11}^E \sigma_{11} + d_{13} E_3 \\ D_3 &= (d^T)_{31} \sigma_{11} + \epsilon_{33}^\sigma E_3, \end{aligned} \quad \text{Eq. 1}$$

where ε_{11} is the strain tensor component in the 1-direction, σ_{11} is the corresponding component of the work-conjugate stress tensor, D_3 is the electric displacement in the 3-direction, E_3 is the electric field in the 3-direction, d_{13} is the piezoelectric coupling coefficient, s_{11}^E is the complex mechanical compliance of the material measured at zero electric field. For the simplified 1D, plane-stress problem at hand, s_{11}^E reduces to the inverse of Young's modulus of elasticity of the piezoelectric material. ϵ_{33}^σ is the complex permittivity measured at zero stress.

Due to the coupled electromechanical behavior of piezoelectric materials, the electrical impedance of the piezoelectric sensors is directly related to the mechanical impedance of the host structure, Z_{st} , as follows [9]

$$Z(\omega) = \left[i\omega \frac{bl}{h} \left(\frac{d_{13}^2}{s_{11}^E} \left(\frac{\tan(kl)}{kl} \left(\frac{Z_{pzt}}{Z_{pzt} + Z_{st}} \right) - 1 \right) + \bar{\epsilon}_{33}^\sigma \right) \right]^{-1}, \quad \text{Eq. 2}$$

where $Z_{pzt} = -iblh \left(s_{11}^E \omega \frac{\tan(kl)}{kl} \right)^{-1}$ is the piezoelectric sensor short circuit impedance, where $k = \omega \sqrt{\rho \bar{s}_{11}^E}$ is the wave number, ρ is the density of the piezoelectric material, b , h and $2l$ are the piezoelectric patch width, thickness and length, respectively.

Because this method is based on vibration the sensitivity of the measurements is dependent on the frequency range used. For a defect to be detected the wavelength of the excitation signal needs to be smaller than the characteristic length of the defect [19]. To achieve higher sensitivity using the impedance based method higher frequency excitations should be used. In work done by Peairs et al. the use of preselected frequency ranges based on the free response of the piezoelectric sensors [20]. Based on this work, they concluded that both the characteristics of the piezoelectric sensor and the part are important for determining the optimal frequency range.

The use of electromechanical impedance measurements has been demonstrated in a variety of structural applications. Park et al. used this technique for applications such as bridge sections, pipe joints, and reinforced concrete walls [21]. Other studies have used impedance measurements to detect defects in both real world conditions and laboratory environments [22 23].

The authors hypothesize that electromechanically impedance measurements may be particularly well suited for in-situ monitoring of AM parts. The authors' previous work has demonstrated the potential for this technique to be used on fully fabricated parts [SFF piezo]. The use of the technique in-situ shares many of the same benefits such as being cost effect (i.e no radiation source needed), time efficient (i.e. each sweep takes seconds to run), and the ability to detect changes in material properties. The features of impedance based measurements allow it to fit many of the needs identified in section 1.2. By using high frequencies, small defects can be detected layer-by-layer as the part is fabricated. Further, because the method is able to detect changes throughout the volume of the part, material changes that might occur in already fabricated layers can be detected.

3. Method

To utilize impedance based techniques for in-situ inspection of AM parts the authors propose a system where an initial set of control parts is used to set a baseline for detecting defects. In this system several copies of the designed part are printed and monitored using the impedance based techniques. For each layer where inspection is desired the signature is recorded. These control parts are then tested using nondestructive and destructive techniques to ensure that they were properly fabricated and meet all design requirements. The signatures from these validated parts are then used to create a set of baseline signatures. Subsequent parts are monitored using these impedance based techniques and are compared to the baseline signatures. Any defects that occur will alter the signature resulting in a difference from the baseline that can be detected. For this method to be applicable the hypotheses presented in Section 1 need to be validated.

3.1 Test specimen Design and Fabrication

As previously presented in Section 1 this study sought to validate three base hypotheses:

1. For a single part at a given layer, the sensors will be able to repeatedly measure the same signature.
2. For a single part, the sensors will be able to detect the change from one layer to another. This change will be greater than the signature variation in a single layer.
3. While being fabricated, all parts will have similar signatures until the defects occur. After the defects are introduced, the sensors will be able to detect differences in the parts' signatures.

To investigate these hypotheses, the authors designed three test parts, (i) a control (Figure 3a, “C”), (ii) a large rectangular prism cavity (Figure 3b, “S”), and (iii) a triangular prism cavity (Figure 3c, “R”). Each part also contained a small cavity at its base for embedding the piezo-ceramic sensor/actuator. The test parts have overall dimensions of 35mm x 19mm x 15mm. The thickness of the wall containing the defects is 1mm. The “S” defect is 33mm x 17mm x 9.5mm for a total volume of 5330mm³ (53.4% of total volume) and a per layer volume of 16.8mm³ (0.17% of total volume). The “R” has a right triangular cross section with sides 33mm and 9.5mm and a depth of 17mm. The total volume of the defect is 2665mm³ (26.7% of total volume) and the smallest layer change is 0.027 mm³ (0.00027% of total volume). The piezos are embedded after 2.5mm of the parts have been printed and the defects begin after 4.5mm.

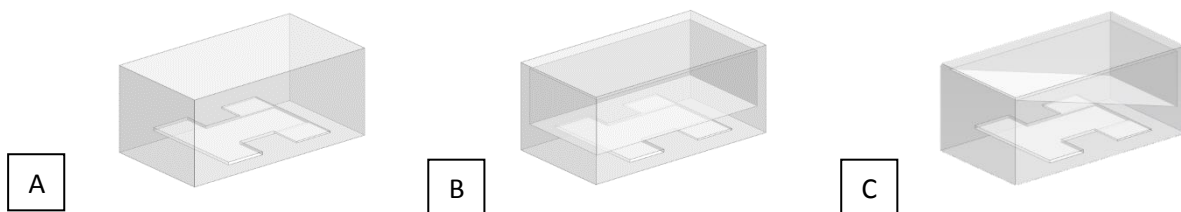


Figure 3. Test parts A) Control sample “C”, B) Rectangular prism cavity “S”, C) Triangular prism cavity “R”

To minimize the potential variation from naturally occurring defects in the printing process as well as from part damage during embedding the design of the test parts was kept as straightforward as possible. This allowed for simple visual inspection to be performed during fabrication to ensure that the parts were being fabricated as expected. The small lower cavities are open and are designed for support material to be removed to allow the piezos to be embedded in the parts. The defect cavities are enclosed to allow the parts to be cleaned after fabrication without removing the support material contained inside the cavities. This allows the total mass of

the part to remain constant while the difference in composition between model and support material changes. The large rectangular cavity is designed to cause a defect with a constantly increasing size, while the triangular cavity will cause a linearly increasing void size. The goal of this linearly increasing defect is to allow for a more precise determination of the minimum detectable defect size.

The parts were printed on a Connex350 printer using VeroWhite+ material and a matte finish. This process was chosen due to the ability to easily mount and access the sensors. The process also has a high resolution, 300 x 600 DPI and 0.03mm layers, which allows for measuring the effect of smaller amounts of material being added. The support material also has similar density to the model material meaning that the effect of a stiffness change without a mass change can be investigated. The primary drawback of the Polyjet process is the limited material selection. The model material is a photopolymer that is less rigid than materials available on other processes, in particular those on metal based systems. Since the transmission of vibration through a part is directly linked to the stiffness of the material this lack of rigidity has the potential to reduce the effective range and sensitivity of the sensors. The support material is very soft and has the potential to act as a large dampener, absorbing the vibrations generated by the piezo-ceramics and further reducing the sensitivity of the sensors. Despite these material limitations the Polyjet process provides a good testbed since the move to more ridged materials would be expected to improve the performance of the sensors in many cases. The test parts were arrayed in a three-by-three grid on the build tray, with one of each type of sample design in every row and column, as shown in Figure 4. The parts were printed until 2.5mm , at which the print was paused, support material was removed from the cavities, and the piezo-ceramic sensors were placed inside and bonded to the part with an adhesive. Before embedding, copper tape was attached to the piezos to provide connection points for measurements.

To minimize variation between sample measurements, each piezo used was cut from the same sheet. Leads were soldered to the ends of the copper tape to provide reliable attachment points. The print was then resumed, with measurements being taken at the layers as shown in Table 1. To allow measurements to be taken consistently the authors paused the build at each listed layer before taking measurements. This was to avoid any changes that could be caused by the print head depositing more material while a measurement was being taken. While the pause and measurement operation was performed manually in this study, it could be automatically programmed into the system to provide interference free in-situ monitoring. In addition to the measurements taken in-situ, the final parts were measured on the build tray, after being removed from the build tray (but before having excess support material removed) and after having been cleaned from support material.

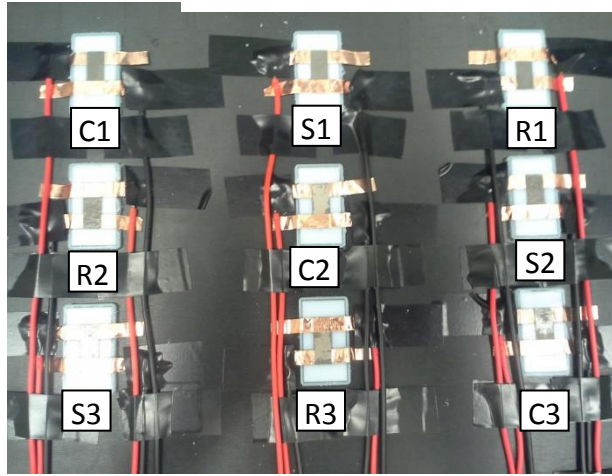


Figure 4. Test parts with piezos embedded and layout of the test parts. The letter indicates the type of part (e.g. “C” for control, “S” for the rectangular prism, and “R” for the triangular prism. The number indicates the sample number for each part. In this case three samples of each type were printed.

Table 1. Part layers where measurements were taken. For each layer, the volume of model material in each part is shown. The right column shows the percentage difference between the defect parts and the control at each layer, indicating the relative size of the defect

Layer	Volume mm ³			Volume %	
	C	S	R	S	R
150	2294	2294	2294	100.0%	100.0%
160	2494	2494	2494	100.0%	100.0%
198	3252	3033	3247	93.3%	99.9%
208	3451	3064	3437	88.8%	99.6%
218	3651	3095	3622	84.8%	99.2%
228	3850	3127	3801	81.2%	98.7%
238	4050	3158	3975	78.0%	98.2%
248	4249	3189	4144	75.0%	97.5%
268	4648	3251	4465	69.9%	96.1%
288	5047	3314	4766	65.7%	94.4%
318	5646	3407	5176	60.4%	91.7%
348	6244	3501	5539	56.1%	88.7%
398	7242	3657	6037	50.5%	83.4%
448	8239	3813	6403	46.3%	77.7%
498	9237	3969	6636	43.0%	71.8%

3.2 Analysis techniques

In this study, the authors situated the analysis in a supervised learning context, where differences in the impedance signatures of fabricated parts against a baseline signature from a known, defect free part are compared. Two of the control samples were used to establish the baseline. The third control sample was used to validate this baseline.

To validate the hypotheses put forth in section 1 three steps were needed, (i) to determine the repeatability of measurements for a single part on a single layer, (ii) to determine the change in a single part between layers, (iii) to determine the difference between parts on the same layer.

Determining the repeatability of the measurements of a single part on the same layer establishes a baseline noise threshold. This baseline also indicates whether or not there is significant interference from the machine between measurements since the authors' previous work has shown good repeatability on fully fabricated parts. To achieve this, three measurements were taken of each part at each layer and the signatures were compared at each frequency to obtain maximum and average deviations for each part. After this the three measurements are added together and all impedance signatures are shifted vertically such that their average value (excluding impedance peaks), match to compensate for any inconsistency in the connectors' resistivity (e.g., due to variations in soldering and wire length).

To quantify the difference in signatures between layers, a damage metric defined as

$$RMSD = \sqrt{\sum \frac{(Z_D - Z_{BL})^2}{Z_{BL}^2}} \quad (2)$$

Where Z_D is the real component of the impedance signature of the part being tested, and Z_{BL} is the real component of the baseline impedance signature, and n is the total number of data points in the impedance signature was used. This metric was used in two ways, (i) to compare a single part to itself in subsequent layers and (ii) to compare different parts to each other in the same layer. In the first case, the signature of the first measured layer is used as the baseline and each subsequent layer is compared to this first layer to determine an overall change in the part. This metric is also used to compare each measured layer to the layer immediately preceding it to determine the change between layers. In the second case, the signatures of the first two control samples are averaged together and used as the baseline. The third control sample is used to verify the baseline value and the other samples are all compared to this baseline. Since each sample is designed to be identical before the defect is introduced the initial baseline difference can be used to calibrate for natural variation between the piezo. This was to account for any difference that might exist due to factors such as differences in the piezoceramics, mounting, or build tray location.

4. Results

4.1 Evaluating Repeatability

In order to perform in-situ measurements it was necessary to determine if the machine would cause interference between measurements and what the background noise level for variation was. As stated in hypothesis 1, it was necessary to test if the machine was causing the measurement of a single part and layer to vary from one moment to another. Figure 5a shows a typical example of a set of three measurements taken from layer 150 of a single control sample, in this case C1. The average deviation of this set of measurements was 0.167Ω , indicating strong repeatability. Based on this, minimal machine interference can be expected between measurements, while some bias may occur, it will be consistent across measurements. The highest deviation was found to be 7.32Ω in layer 448 of part R3. As shown in Figure 5b, this is mostly the result of a linear offset occurring between measurements. A linear offset will be caused by an increase in the total resistance of the system usually attributable to something such as an increased connection resistance in the case of a poor wire connection. This offset can be corrected for by subtracting the mean of each trace to normalize the data. Overall, the samples showed good repeatability of measurements throughout all of the layers tested. Of note are the higher deviations for R1 and R3, indicating potential challenges in comparing these measurements. This is most likely due to errors that occurred while embedding and is discussed in more detail in Section 4.3.

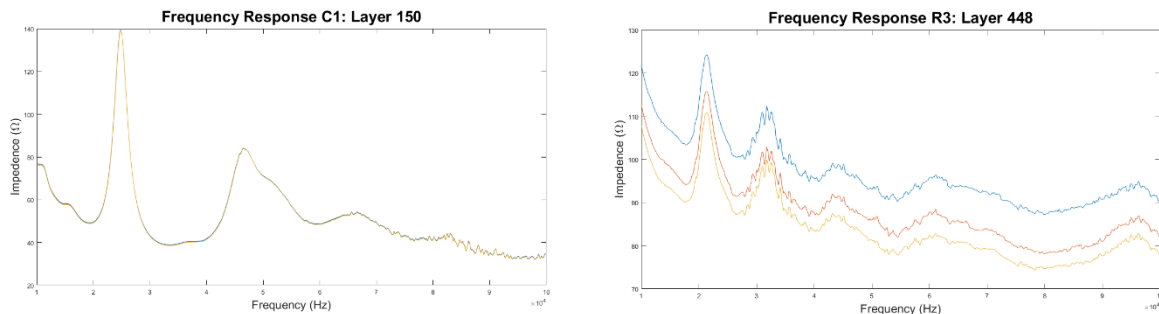


Figure 5. Part signatures sample parts. On the left is a typical measurement deviation shown for Control 1 (maximum deviation = 0.49Ω). On the right is an example of the worst case deviation observed, in this case for Ramp 3 (maximum deviation = 7.3Ω).

Table 2. Repeatability measurements for each sample taken across all layers measured. Of note are the particularly high numbers for R1 and R3.

Part	Max Deviation (Ω)	Average Deviation (Ω)
C1	2.524	0.271
C2	1.224	0.089
C3	0.891	0.054
R1	3.862	0.855
R2	0.735	0.140
R3	7.323	1.210
S1	1.211	0.111
S2	0.824	0.091
S3	1.241	0.055

4.2 Evaluating Change in a Single Part Between Layers

To evaluate the proposed technique's ability to detect changes between layers in a single part, as proposed in the second hypothesis (Section 1), the authors compared both (i) the total change from the first layer to the measured layer, and (ii) the change between layers for a single sample. This experimental approach provided a measure of total change and of relative change between measured layers.

To compare the total change the authors used a single part (C1) and selected the signature of the first measured layer (layer 150). This layer was set as the reference layer to which all other layers were compared. This layer was 3.42mm into the part and was chosen to allow the piezo to be completely enclosed and secured by model material. This layer occurs before any defects are introduced into the part. When comparing the total change in signature from the reference layer, it is observed that all layers showed a significant difference, far above the noise threshold. This indicates that changes could easily be detected. Figure X shows the total difference from the reference layer for part C1. Increasing difference in signatures can be seen as more layers are added to the part. The smallest difference that was measured was between 10 layers (0.3mm) with the added volume being 199.5mm³. A sample of the measured signatures is shown in Figure X. A slight shift (left) can be seen in the peaks of the signatures as more layers are added to the part.

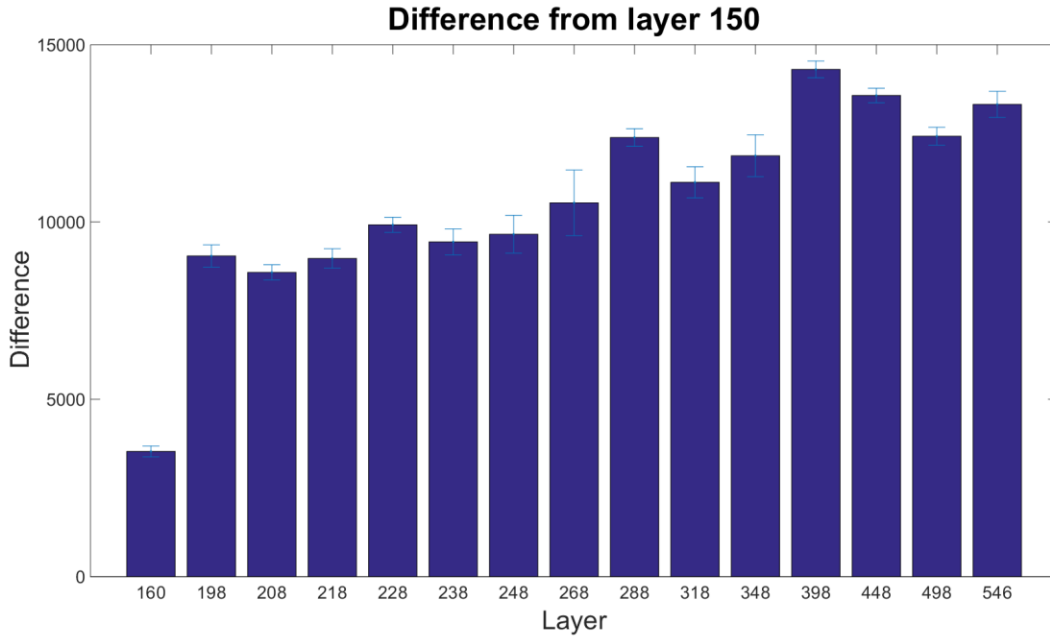


Figure 6. Total difference in signatures of part C1 from each measured layer to the reference layer (150). Increasing difference can be seen as more material is added to the part.

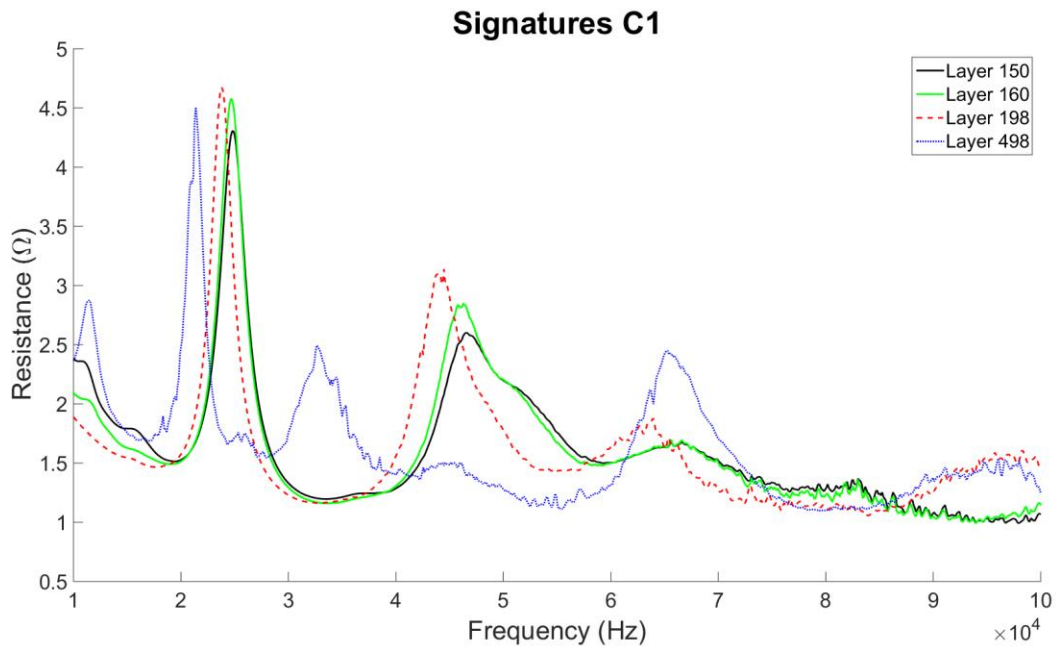


Figure 7. Select signatures of part C1. Layers 150, 160, 228, and 498 are shown. A slight shift (left) of the peaks can be observed with increasing layers.

It is important to note that while two layers may have a similar total magnitude of difference from the reference layer, their signatures might be significantly different from each other. To illustrate this, imagine a sine wave as the reference layer. While both a leftward and a rightward shift of the signature by five degrees causes the same magnitude of change, the two signatures are indicating very different changes, and the difference between the two shifted signatures is greater than the difference from the reference part. To evaluate this, the signature of each layer in C1 was compared to the signature of the layer before it. Figure 8 shows the difference of each layer from the layer before it; in each case the difference is well above the noise threshold. Because the separation of measured layers is not constant throughout the print, it is important to look at the effects of volume of material added on the measured difference. In a direct comparison between the addition of 10 and 20 layers the difference from adding 20 layers will be inflated due to more material being added. Since each layer has a cross section that contains the same area of material, two different measurements can be equally compared by normalizing to the number of layers added.

Figure 9 shows the difference in signatures for C1 between layers divided by the number of layers added. In this normalized graph, a trend toward decreasing sensitivity can be seen to start occurring around layers 268 to 288. At the earlier layers the signatures tend to change more significantly, as more material is added there tends to be less movement and variation in the signatures. This explains the large variation and unpredictability in the difference of the earlier layers compared to the more stable trend of the later layers. This trend can probably be attributed to the increased amount of total mass in the part. As more material is added the volume/mass of each added layer remains constant, while the total mass of the part continues to increase. This causes the percent change of the part to decrease with each layer. In addition the new material is further away from the sensor. As distance from the sensor increases the ability to detect changes will decrease. .

The results of this test show that the difference between layers in a single part can be detected and that this difference is above the variation threshold found when verifying the first hypothesis. This method is able to successfully detect increasing change from a reference layer and is also able to clearly detect change between layers as proposed in the second hypothesis. The diminishing layer to layer difference indicates that the hypothesis is valid only with a certain range of part masses. A sufficiently large system may result in a sensitivity drop below the minimum detection threshold.

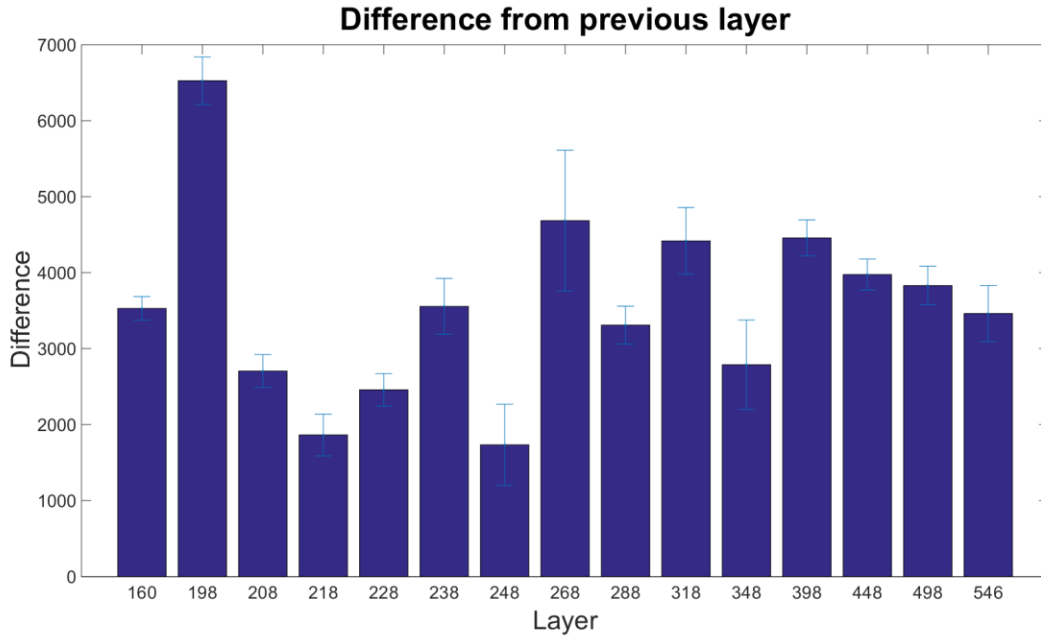


Figure 8. Difference in signature of each measured layer to the measured layer before it.

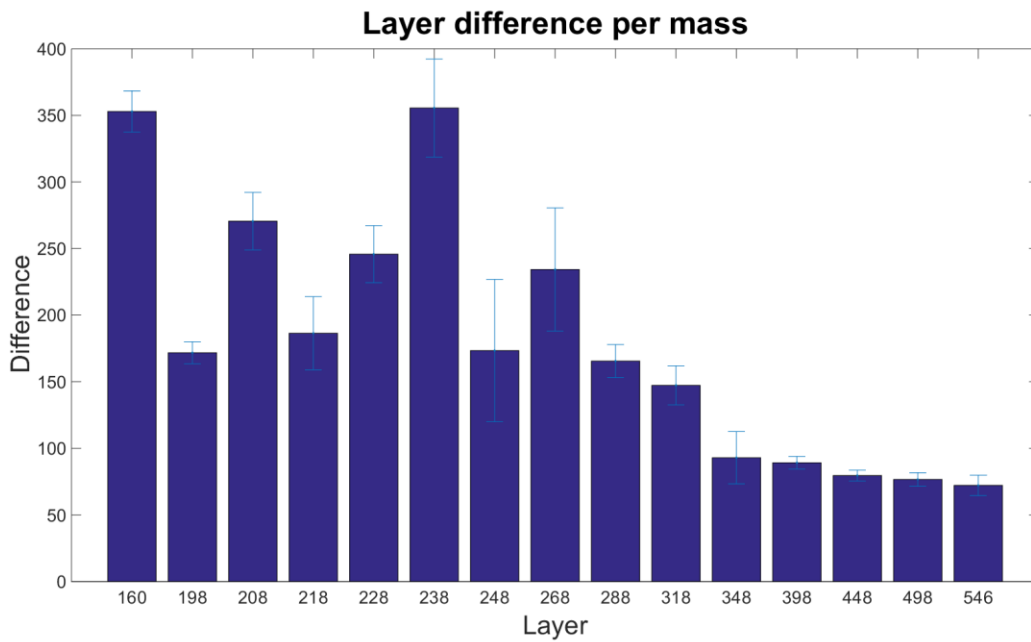


Figure 9. Difference in signature after scaling for the mass difference being measured. After the initial variation it can be seen that a trend toward decreasing sensitivity with added part mass begins to occur.

4.3 Defect Detection Comparison Across Parts

To determine if defects could be detected compared to a reference “good” part, a baseline measurement was created by averaging the measurements of two of the control samples, C1 and C2 (Section 3.2). Due to small variations in the piezos and in their mounting some difference exists between the baseline and the test parts before the defects are introduced. To calibrate the measurements, the difference found in the first measurement is subtracted from the subsequent measurements. This was done to minimize any bias due to the sensor. Figure 10 is a color graph showing the difference magnitude (RMSD) for each part across all layers. Darker blues indicate less difference between the part and the baseline. Bright yellows indicate increased difference from the baseline.

It can be seen that the control samples maintain a relatively small difference from the baseline while the samples with the defects have a small initial difference, but quickly show a much larger difference from the baseline. The red line indicates where the defect occurs and the circled area shows where the defect can be detected. For the rectangular prism void the defect can be detected at layer 198 (defect volume 219 mm³, corresponding to a 6.7% volume fraction of the total part). As the defect continues to grow, it can be seen that the difference between the defect parts and the control parts continues to trend towards increasing, with the correlation between similar parts being fairly close.

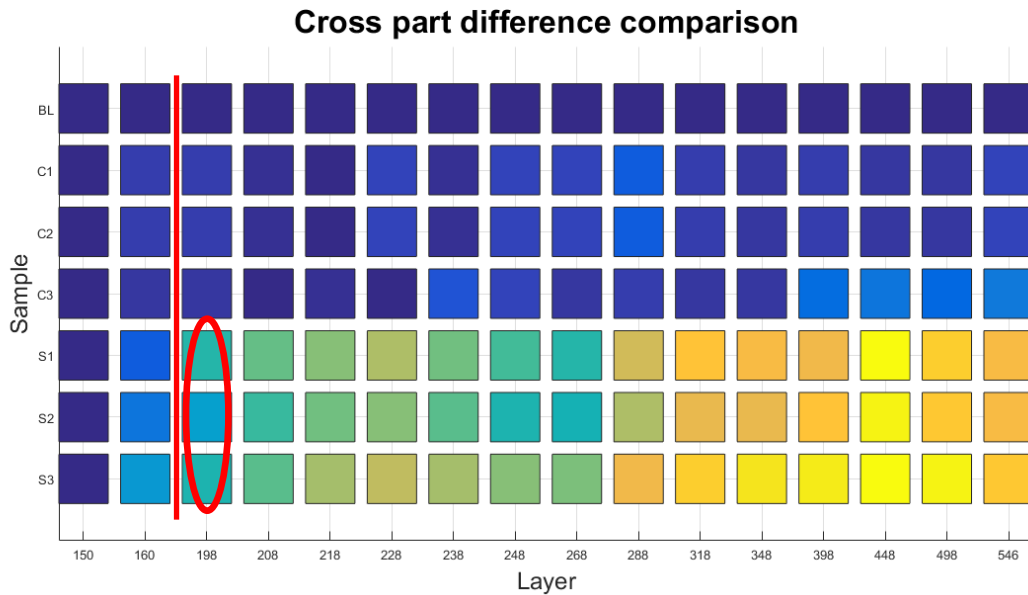


Figure 10. Difference between the baseline (average of C1 and C2), the control samples, the triangular prism void (R), and the rectangular prism void (S) for each measured layer. The samples with defects can be seen to increase in difference while the controls remain approximately the same. The defect in the S samples can be detected in layer 198, the first measured layer after the defect is introduced at layer 186. The R defect can be detected in layer 218.

In looking at the initial difference for the ramp samples, it was found that R1 and R3 had a very high initial difference. Upon investigating the signatures, shown in Figure 10, it is clear that there is a significant difference in these samples compared to the control. Due to the important of the physical bond between the part and the sensor, the potential for damage to the piezo, and the difficulty in completely removing support material and attaching the sensor it is likely that this error occurred as part of the embedding process. Due to the apparent defect in embedding, these samples were excluded and only R2 is shown for the difference comparison in subsequent layers.

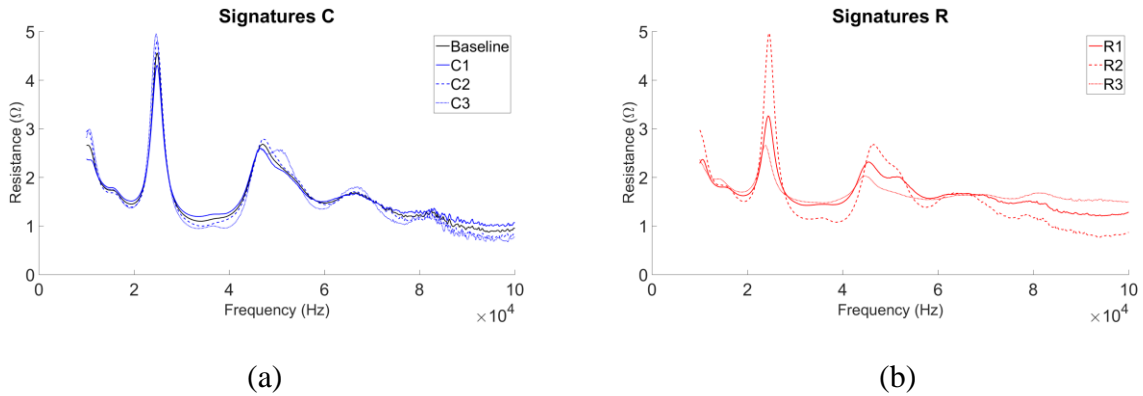


Figure 10. a) Comparison of the measured signals of the controls samples. Signatures are similar and closely clustered. b) Comparison of the measured signals of the triangular prism samples. The R1 and R3 samples show a significant difference from the expected signature. This is likely due to a failure in the embedding process.

The remaining sample (R2), as expected, showed a smaller degree of difference than the previous rectangular void samples (S1,S2,S3), due to the smaller size of the defect. In the triangular prism sample, the defect could be accurately detected in layer 218, corresponding to a defect asize of 29mm³ (0.8% volume fraction of the total part). Before this, the difference was not significant enough to determine with certainty that a defect had occurred. After detection, and with increasing defect size, the detected RMSD difference generally continued to increase, but to a lesser level than the rectangular prism samples. Since the triangular prism defect is smaller this result is expected. Figure 12 shows the color chart comparison for the ramp for each layer.

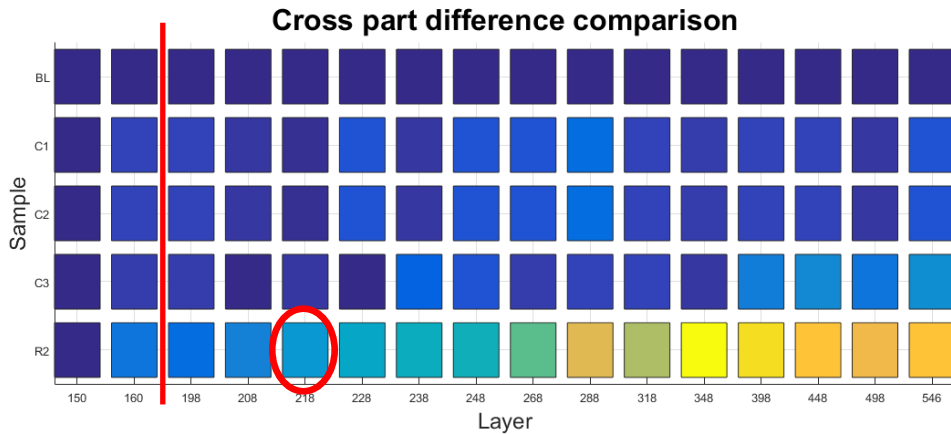


Figure 12. Difference between the baseline, the control samples, and the support samples for each measured layer. The support samples can be seen to increase in difference while the controls remain approximately the same. The defect can be detected in layer 218.

5.0 Closure and future Work

The authors have shown that piezo-ceramic sensors can be used in-situ to monitor parts. In this study three hypotheses has been verified, the repeatability of the same measurement, the detection of changes in a single part between layers, and the detection of differences between parts after a defect is introduced. For the first hypothesis, within the same part and layer, the results were very repeatable with the average deviation of the control sample's damage metric being only 0.27Ω (Table 2). This showed that there was minimal interference from the machine between measurements, a requirement for being able to perform high sensitivity in-situ measurements.

For the second hypothesis, the method was able to detect changes occurring between one layer to another. The detected resolution was ten layers (0.3mm), corresponding to a volume change of 199.5 mm^3 (4.2% volume fraction). Much smaller changes should be detectable, however this was the smallest increment that was tested in this study. In general, the difference from the base layer tended to increase as more layers were added to the part. Sensitivity of the measurements was also noted to decrease as more material was added to the part. While these trends are not conclusive these results reinforce initial hypothesis on the behavior of the system.

For the third hypothesis, the sensors proved to be less effective at detecting defects between parts in-situ than in similar tests on completed parts. The smallest defect that was detected in-situ was 29mm^3 (0.8% volume fraction), compared to defects as small as 8mm^3 in fully fabricated parts. The authors hypothesis that this is due in part to the extra supporting material around the part, the extra mass in the system due to being fixed to the build tray, and the potential for the location on the build tray to have an effect on the signature. Despite the somewhat reduced sensitivity, the

in-situ method was still able to reliably detect defects in the parts as they occurred. Refinements to the technique and analysis should be able to allow for the detection of smaller defects.

The parts in this study were fabricated on a Connex 350. While this system provides a convenient test bed for validating the concept of impedance based in-situ monitoring, the materials available on this system are expected to perform poorly. Due to the high damping of the support material on this system it is expected that the sensitivity of the method could be improved. Detection of defects is dependent of the transmission of vibration through the part; therefore parts made out of stiffer materials can be expected to perform better with this method. In particular, the authors hypothesize that metal based AM systems will perform significantly better and will allow for the detection of smaller defects.

To more fully qualify the sensitivity and size of defects that can be detected in-situ further work needs to be done investigating smaller step sizes. In addition, the authors plan to conduct in-situ measurements on an FDM system with the hypothesis that the stiffer support material may provide less dampening and result in more sensitive detection abilities. Other future work includes the validation of these methods on metal systems where the much greater stiffness is expected to improve the sensitivity of the method. To further refine the sensitivity of the method more sophisticated analysis techniques than RMSD are being investigated. One example is the use of peak detection and comparison to more precisely isolate the important sections of the signature.

Acknowledgements:

This material is based upon work supported by the national science foundation under grant #1446804: “CPS Synergy: Collaborative Research: Cyber-Physical Approaches to Advanced Manufacturing Security” Any opinions, findings, and conclusions or recommendations expressed in this material are those of the author(s) and do not necessarily reflect the views of the National Science Foundation.

References

- [1] NIST, 2013, “Measurement Science Roadmap for Metal-based Additive Manufacturing,” http://www.nist.gov/el/isd/upload/NISTAdd_Mfg_Report_FINAL-2.pdf, prepared by Energetics Incorporated, May.
- [2] Rolls Royce, 2015, “High-Powered Trent XWB-97,” *Rolls Royce Media Insights* <http://www.rolls-royce.com/media/insights/simon-burr.aspx>, August 31.
- [3] RUAG, 2014, “RUAG pioneers 3D printing for space,” *RUAG Media Release* <http://www.ruag.com/group/media/media-releases/news/ruag-pioneers-3d-printing-for-space/d39b1226395457f3362a92216064fa1e/> August 31.
- [4] Stratasys, 2015, “Additive Manufacturing for Aerospace: FAA-Approved Air Duct for ‘Flying Eye Hospital’ Produced in Just Days,” <http://blog.stratasys.com/2015/03/05/3d-printed-air-duct-flying-eye-hospital/> March 5.
- [5] A. Plessis, S. Roux, J. Els, G. Booysen, and D. Blaine, 2015, “Application of microCT to the non-destructive testing of an additive manufactured titanium component,” *Case Studies in Nondestructive Testing and Evaluation*, vol. 4, pp. 1-7, Nov. 2015.
- [5] L. D. Sturm, C. B. Williams, J. Camelio, J. White, and R. Parker, 2014, “Cyber-physical Vulnerabilities in Additive Manufacturing Systems,” *International Solid Freeform Fabrication Symposium*, Austin, TX., August 4-6.
- [6] S. Berumen, F. Bechmann, S. Lindner, J.-P. Kruth, T. Craeghs, “Quality control of laser and powder bed-based Additive Manufacturing (AM) technologies,” *Phys. Procedia* 5 (Part B) (2010) 617–622.
- [7] T. Furumoto, T. Ueda, M.R. Alkahari, A. Hosokawa, “Investigation of laser consolidation process for metal powder by two-color pyrometer and high-speed video camera,” *CIRP Ann. Manuf. Technol.* 62 (1) (2013) 223–226 (PubMed PMID: WOS:000322555800056).
- [8] T. Furumoto, T. Ueda, N. Kobayashi, A. Yassin, A. Hosokawa, S. Abe, “Study on laser consolidation of metal powder with fiber laser—evaluation of line consolidation structure,” *J. Mater. Process. Technol.* 209 (18–19) (2009) 5973–5980.
- [9] T. Watkins, H. Bilheux, A. Ke, A. Payzant, R. Dehoff, C.E. Duty, et al., “Neutron characterization for additive manufacturing,” *Adv. Mater. Process.* 171 (3) (2013) 23–27.
- [10] S. Everton, M. Hirsch, P. Stravroulakis, R. Leach, A. Clare, “review of in-situ process monitoring and in-situ metrology for metal additive manufacturing,” *J. Materials and Design*, vol. 95, pp. 431-445, 2016
- [11] P. Lott, H. Schleifenbaum, W. Meiners, K. Wissenbach, C. Hinke, J. Bültmann, “Design of an Optical system for the In Situ Process Monitoring of Selective Laser Melting (SLM),” *Physics Procedia*, vol 12, pp. 683-690, 2011
- [12] P. Rao, J. Liu, D. Roberson, Z. Kong, C. Williams, “Online Real-Time Quality Monitoring in Additive Manufacturing Processes Using Heterogeneous Sensors,” *J. Manuf. Sci. Eng.*, vol. 137, pp.061007-061007-12, 2015
- [13] M. Albakri, L. Sturm, C. Williams and P. Tarazaga, “Impedance-based Non-destructive Evaluation of Additively Manufactured Parts” *Rapid Prototyping Journal*” Pending Publication

- [14] J. Waller, B. H. Parker, K. L. Hodges, E. R. Burke, and J. L. Walker, 2014, “Nondestructive Evaluation of Additive Manufacturing: State-of-the-Discipline Report,” NASA/TM-2014-218560, November.
- [15] ASTM, “Committee F42 on Additive Manufacturing Technologies,” <http://www.astm.org/COMMITTEE/F42.htm>
- [16] G. Park, H. Sohn, C. R. Farrar, and D. J. Inman, “Overview of piezoelectric impedance-based health monitoring and path forward,” *Shock Vib. Dig.*, vol. 35, no. 6, pp. 451–464, 2003.
- [17] C. Liang, F. P. Sun, and C. A. Rogers, “Coupled Electro-Mechanical Analysis of Adaptive Material Systems — Determination of the Actuator Power Consumption and System Energy Transfer,” *J. Intell. Mater. Syst. Struct.*, vol. 5, no. 1, pp. 12–20, Jan. 1994.
- [18] V. Giurgiutiu and A. N. Zagari, “Characterization of piezoelectric wafer active sensors,” *J. Intell. Mater. Syst. Struct.*, vol. 11, no. 12, pp. 959–976, 2000.
- [19] D. J. Leo, *Engineering analysis of smart material systems*. Hoboken, N.J: Wiley, 2007.
- [20] D. M. Peairs, P. A. Tarazaga, and D. J. Inman, “Frequency Range Selection for Impedance-Based Structural Health Monitoring,” *J. Vib. Acoust.*, vol. 129, no. 6, p. 701, 2007.
- [21] G. Park, H. Cudney, and D. Inman, “Impedance-Based Health Monitoring of Civil Structural Components,” *J. Infrastruct. Syst.*, vol. 6, no. 4, pp. 153–160, 2000.
- [22] H. Wang and L. Zou, “Interfacial effect on the electromechanical behaviors of piezoelectric/elastic composite smart beams,” *J. Intell. Mater. Syst. Struct.*, vol. 24, no. 4, pp. 421–430, Mar. 2013.
- [23] V. G. M. Annamdas and C. K. Soh, “Application of Electromechanical Impedance Technique for Engineering Structures: Review and Future Issues,” *J. Intell. Mater. Syst. Struct.*, vol. 21, no. 1, pp. 41–59, Jan. 2010.